Biogas-fed solid oxide fuel cell (SOFC) coupled to tri-reforming process: Modelling and simulation

Flavio Manenti [a,**], *Renato Pelosato* [a,*], *Paolo Vallevi* [a], *Andres Ricardo Leon-Garzon* [a], *Giovanni Dotelli* [a], *Antonio Vita* [b], *Massimiliano Lo Faro* [b], *Gaetano Maggio* [b], *Lidia Pino* [b], *Antonino S. Aricò* [b]

[a] *Politecnico di Milano, Dipartimento di Chimica, Materiali e Ingegneria Chimica "Giulio Natta", Piazza Leonardo da Vinci 32, 20133 Milano, Italy*

[b] *CNR-ITAE, Istituto di Tecnologie Avanzate per l'Energia "Nicola Giordano", Via Salita S. Lucia sopra Contesse 5, 98126 Messina, Italy*

Received 13 March 2015
Received in revised form
3 August 2015
Accepted 16 August 2015
Available online 9 September 2015

Introduction

Due to several economic, environmental and societal factors, the dependence of energy production and transportation on fossil fuels has proven to be unsustainable in the long term [1]. As a result, great attention has been paid to the utilization of renewable energy sources and to efficiency improvements.

Hydrogen is one of the most promising renewable energy carrier, as it is versatile, clean and ubiquitous up to the point that the term "hydrogen economy" has been coined to indicate a post-fossil-fuel world [2]. Traditionally, hydrogen is produced from fossil sources, through steam reforming (SR) or partial oxidation (POX) of hydrocarbons (usually methane), or coal gasification. It can also be obtained from non-fossil sources through electrolysis of water, biomass gasification and reforming of bio-fuels as ethanol or biogas [3–5]. Indeed, biogas can be obtained from various biomasses and processes such as degradation of urban and industrial waste, landfills,

* *Corresponding author*. Tel.: +39 02 2399 3232; fax: +39 02 7063 8173.
** *Corresponding author*. Tel.: +39 02 2399 3273; fax: +39 02 7063 8173.
E-mail addresses: flavio.manenti@polimi.it (F. Manenti), renato.pelosato@polimi.it (R. Pelosato).

co-digestion of zootechnical effluents, agricultural wastes and energy crops [6]. It consists of a mixture of methane (40–70% vol.) and carbon dioxide (30–60% vol.) and traces of other gases (1–5% vol.) like hydrogen (0–1% vol.) and hydrogen sulphide (0–3% vol.). Nowadays biogas is mostly used to pro-duce heat and electricity through power turbines and internal combustion engines, even though employing biogas in such systems can sometimes result in low electrical conversions, high levels of noise, maintenance problems and pollutant emissions [7]. In this context, hydrogen can play an important role, allowing to employ biomass-derived fuels in more efficient power generation systems such as fuel cells (FCs) [8–11].

In particular, solid oxide fuel cells (SOFCs) are considered the simplest fuel cell concept available on the market, as there are only two phases involved in the system (gas and solid); they operate in temperatures ranging from 600 °C to 1000 °C and thus are characterized by high reaction rates. Due the high operation temperature, solid oxide fuel cells allow the integration of all the fuel processing stages, from purification to conversion (i.e. reforming), and also the co-generation of heat at high temperatures [8]. A purification step is necessary to remove poisonous agents such as H_2S, NH_3, halides, siloxanes and other species that could affect the performance of the reforming catalyst or the nickel anode [12].

Among biogas reforming options, both Dry Reforming (DR) and Steam Reforming (SR) present issues related to the severe operating conditions that lead to deactivation of the catalyst, caused by sintering of the metallic phase and sup-port [13] and by coke deposition [14]. In addition, the request of an external heat source to supply the endothermic re-actions and to preheat the reforming agent (steam) reduces the overall efficiency of the fuel processor and of the global system (Processor-SOFC) [15,16]. Also the Catalytic Partial Oxidation (CPOX) process has been proposed to produce hydrogen/syngas from biogas; due to its exothermicity, CPOX is considered more promising in terms of energy saving if compared to the SR and DR processes [17,18]. However, CPOX can present several problems, including risk of explosion and hotspot formation, with consequent catalyst deactivation, which results in loss of activity [19,20]. A new catalytic process that may address these issues is called tri-reforming: it simultaneously combines all the above processes in a single step [21]. In such a process, the carbon deposition on the catalyst is circumvented by the presence of water and oxy-gen, and the energy requirements are reduced due to the combination of the two endothermic processes (i.e. dry reforming and steam reforming) with an exothermic one (i.e. partial oxidation). An important benefit of the tri-reforming process is the inherent flexibility of the system itself; in fact, by simply modifying the process variables such as temperature, O_2/CH_4 and H_2O/CH_4 ratios, it is possible to achieve an auto-thermal operation [22]. In the same way, such modifications allow to modulate the syngas final composition. Therefore, it can be used for the production of chemicals (such as methanol or dimethyl ether) [23], syn-thetic ultraclean fuels (through the Fischer–Tropsch syn-thesis [24]) or the generation of electric power (through a fuel cell, such as in the case of the present work). Moreover, as explained earlier, the tri-reforming process allows a safer operation of the catalyst, as the presence of both oxygen and water greatly reduces carbon deposition, increasing its life time. Additionally, the milder thermal operation also allows to safeguard the catalytic material from sintering. The catalytic systems used in the Tri-reforming process must be able to ensure high CH_4 and CO_2 conversions with elevated H_2 yield; generally, these requirements are fulfilled by noble metals (Pt, Rh, Ru) and/or Ni, supported on oxides or mixed oxides promoting strong metal interaction (ceria, zirconia, titanium dioxide, ceria–zirconia, ceria–lanthana) [25–28]. On a system level (Fuel processor/SOFC), it is obvious that steam is the most attractive reforming agent for the biogas-fed SOFC in view of maximizing the power density, although the overall electrical efficiency is lowered due to the high energy requirement of the steam generation. However, the utilization of tri-reforming process can be justified not only for the contribution to the life-time of the catalyst, but also for the mitigation of the endothermicity of the overall system; the heat load decreases thus reducing the amount of steam added. This effect is more appreciable when low O_2/CH_4 (0.1–0.2) and H_2O/CH_4 (0.7–1.5) ratios are used. In this case a catalyst with a good resistance to carbon deposition is required [29]. Moreover, the utilization of O_2/Air does not require significant modification to the system, because an oxy-combustor is generally used to recover heat from anodic exhausts. Additionally, with the tri-reforming the reactor can be stopped and restarted quickly, when the discontin-uous supply of biogas and energy input requires it; this result in the lowest cost/benefit ratio among the reforming processes.

Despite the interest in a combined tri-reformer/SOFC process, limited efforts have been made in literature to study such systems; some authors proposed detailed models but did not provide experimental validation [30], others reported about biogas fed SOFCs with internal reforming, and only few papers report the modelling and experimental validation of externally reformed biogas coupled with SOFC power unit [8,31,32]. The experimental set up and tests under different operative conditions were already developed for such a combined process [7]. As a step forward, the main purpose of the present work is the modelling and simulation of the combined process and the comparison of the numerical results with the available experimental data. In fact, the biogas-fed SOFC and tri-reforming system is quite cumbersome to characterize due to the unavailability of dedicated models in the existing process simulators (e.g., AspenHysys, UniSim, PRO/II). Only recently some basic models for fuel cells have been included in such systems, but they still lack in wide-range validation [33–35]. More-over, systems involving complex kinetics are still very challenging for process-scale simulations and industrial scale-up as well, due to complexities in their formulation and in solving them efficiently with appropriate reliability. This work tries to couple for the first time different process simulation tools to provide a unified picture of the biogas-fed SOFC system.

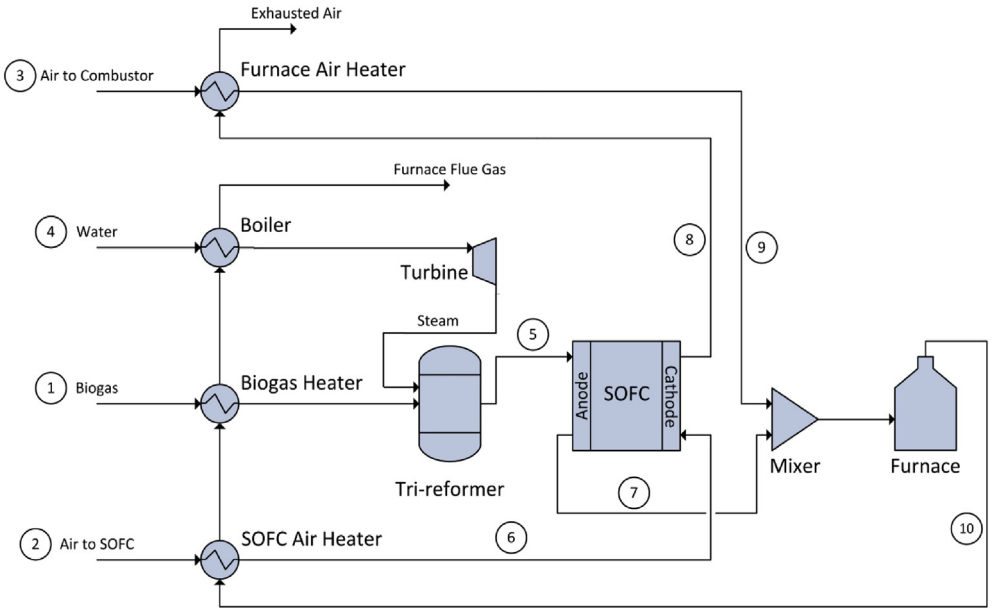

Fig. 1 – Combined tri-reformer/SOFC process flowsheet.

Combined tri-reformer/SOFC process modelling

Fig. 1 depicts the combined process flow sheet: biogas (Stream 1) is fed to a heat exchanger (Biogas Heater) where it is heated to the temperature of the tri-reformer by the flue gas coming from the furnace (Stream 10). The biogas stream is then fed to the tri-reformer where the dry reforming, steam reforming and partial oxidation reactions take place. The reformed biogas (Stream 5), henceforth called "reformed", is sent to the anode of the fuel cell. Meanwhile, air (Stream 2) is sent to a heat exchanger (SOFC Air Heater) where it is heated to the fuel cell temperature (800 °C) by the flue gas from the furnace (Stream 10). The pre-heated air is then directed to the cathode of the fuel cell (Stream 6). In the solid oxide fuel cell the electrochemical reactions of oxygen (present in air) and hydrogen (present in the reformed) take place resulting in two exhausted streams. The first (Stream 7) is the exhausted reformed and is directed to the mixer, while the second (Stream 8) is the exhausted air channelled toward the heat exchanger (Furnace Air Heater) to pre-heat an additional air stream (Stream 3), which is then supplied to the mixer. Both the exhausted reformed (Stream 7) and the pre-heated air (Stream 9) are mixed in the same chamber (mixer) and then supplied to the furnace for the post-burning process. As already mentioned, the flue gas from the furnace (Stream 10) pre-heats air and biogas fed to the SOFC; then it produces steam in the boiler (Stream 4); steam is then expanded in a turbine to produce electricity before being supplied to the tri-reforming reactor.

The simulation of the process was performed using PRO/II® 8.3 software (Schneider Electric Simulation Science); SOFC and furnace operations were instead simulated using ad-hoc models linked to the main simulator, as it will be explained later.

Tri-reformer model

As stated earlier, the tri-reforming process consists of a combination of three catalytic processes in a single step: dry reforming (DR), steam reforming (SR) and partial oxidation (POX), whose reactions are specified below.

$$DR: \quad CH_4 + CO_2 \leftrightarrow 2CO + 2H_2 \quad \Delta H_{298K} = 247.3\ \text{kJ/mol} \tag{1}$$

$$SR: \quad CH_4 + H_2O \leftrightarrow CO + 3H_2 \quad \Delta H_{298K} = 206.3\ \text{kJ/mol} \tag{2}$$

$$POX: \quad CH_4 + \frac{1}{2}O_2 \leftrightarrow CO + 2H_2 \quad \Delta H_{298K} = -35.6\ \text{kJ/mol} \tag{3}$$

The biogas fed to the system has the following composition: $CH_4 = 60\%$, $CO_2 = 40\%$; the tri-reforming process operates at thermodynamic equilibrium conditions, thus a Gibbs reactor is used in the simulation. This reactor solves the set of reactions and the phase equilibria by minimizing the Gibbs free energy, only assuming the mass balance [36]. The reactor temperature is set to 800 °C, and the O_2/CH_4 and H_2O/CH_4 molar ratios were varied between 0.05–0.1 and 0.3–0.7 respectively, as reported in Tables 1 and 2. The selected equation of state is the Soave–Redlich–Kwong (SRK) [37].

Besides, the water gas shift reaction (WGS) and the total oxidation of methane (TOX) can also occur and have been taken into account in the tri-reforming model:

$$TOX: \quad CH_4 + 2O_2 \leftrightarrow CO_2 + 2H_2O \quad \Delta H_{298K} = -880.0\ \text{kJ/mol} \tag{4}$$

$$WGS: \quad CO + H_2O \leftrightarrow CO_2 + H_2 \quad \Delta H_{298K} = -41.09\ \text{kJ/mol} \tag{5}$$

As mentioned above, the main goal of this work is the development of a model that takes in proper account the tri-reforming process and a solid oxide fuel cell (described in the next paragraph). In particular, the main assessment of

Table 1 – Outlet composition of the tri-reforming process with different inlet molar ratio.

Test	Inlet molar ratio			Model outlet composition [mol]		Exp. outlet composition [mol]	
	CH_4/CO_2	O_2/CH_4	H_2O/CH_4	CO	H_2	CO	H_2
#1	1.5	0.10	0.7	0.320	0.522	0.328	0.519
#2	1.5	0.08	0.7	0.324	0.527	0.333	0.522
#3	1.5	0.05	0.7	0.328	0.534	0.337	0.532
#4	1.5	0.10	0.5	0.351	0.527	0.356	0.523
#5	1.5	0.08	0.5	0.354	0.531	0.362	0.529
#6	1.5	0.05	0.5	0.359	0.537	0.372	0.532
#7	1.5	0.10	0.3	0.384	0.525	0.394	0.532
#8	1.5	0.08	0.3	0.387	0.528	0.394	0.531
#9	1.5	0.05	0.3	0.390	0.530	0.398	0.543

such approach is that the composition of the stream from the reforming section, evaluated by using the PRO/II® software, represents the inlet gas fed to the SOFC's anode.

Solid oxide fuel cell model

The electrochemical reactions involved in a solid oxide fuel cell are the following.

$$Anode: \quad H_{2(g)} + O^{2-} \leftrightarrow H_2O_{(g)} + 2e^- \tag{6}$$

$$Cathode: \quad \frac{1}{2}O_{2(g)} + 2e^- \leftrightarrow O^{2-} \tag{7}$$

$$Global: \quad H_{2(g)} + \frac{1}{2}O_{2(g)} \leftrightarrow H_2O_{(g)} \tag{8}$$

An ad-hoc model was developed to simulate the electrochemical behaviour of a SOFC button cell; this modelling allows the calculation of parameters such as the current density, the cell voltage and the gas composition of the outlet stream from both anode and cathode of the fuel cell. The model consists of a non-linear system built up with the operative voltage of the cell $V_{OP}(i)$ as a function of the current density, as described in Eq. (9).

$$V_{OP}(i) = V_{REV} - \eta_{OHM} - \eta_{ACT} - \eta_{CONC} \tag{9}$$

where V_{REV} is the reversible potential, also called open circuit voltage (OCV), given by the well-known Nernst equation:

$$V_{REV} = -\frac{\Delta G_{rxn}}{2F} + \frac{R_g T}{2F}\ln\left(\frac{\left(\frac{P_{H_2}}{P_{Ref}}\right)\left(\frac{P_{O_2}}{P_{Ref}}\right)^{0.5}}{\left(\frac{P_{H_2O}}{P_{Ref}}\right)}\right) \tag{10}$$

The other terms of Eq. (9) are related to the losses inside the whole fuel cell represented by the ohmic losses (η_{OHM}), activation losses (η_{ACT}) and concentration losses (η_{CONC}).

The MS Excel Solver was used to extract the current density value by finding the zeroes of the non-linear equation (Eq. (9)) at each fixed voltage. The obtained current density is then used to calculate the related parameters, like the gas compo-sition in the cathode and anode outlet streams, the power density and the utilization factor. The output values are then passed on to the PRO/II software. The details of the electro-chemical equations used in the model are reported below.

Definitions of the remaining parameters may be found in the Nomenclature.

Ohmic losses

The ohmic losses are directly related to the resistance to the electron flow in the electrodes and the resistance to the ionic flow in the electrolyte. The associated potential loss is calculated as

$$\eta_{OHM} = i \cdot R \tag{11}$$

Table 2 – CH_4 and CO_2 conversion for the tri-reforming process with different inlet molar ratio.

Test	Inlet molar ratio			Model conversion [%]		Exp. conversion [%]	
	CH_4/CO_2	O_2/CH_4	H_2O/CH_4	CH_4	CO_2	CH_4	CO_2
#1	1.5	0.10	0.7	98.4	65.5	99.4	67.6
#2	1.5	0.08	0.7	98.2	67.7	99.4	70.1
#3	1.5	0.05	0.7	97.9	70.1	99.4	74.3
#4	1.5	0.10	0.5	97.6	76.2	99.2	78.3
#5	1.5	0.08	0.5	97.3	78.4	99.2	80.5
#6	1.5	0.05	0.5	96.7	81.5	99.1	84.2
#7	1.5	0.10	0.3	95.8	86.7	99.0	88.9
#8	1.5	0.08	0.3	95.1	88.6	97.6	90.2
#9	1.5	0.05	0.3	93.7	90.8	96.0	93.9

The value of the resistance R can be obtained theoretically, but for a rigorous determination it should be related to the operative conditions (e.g. temperature) and structure (thickness, materials, etc.) of each component of the cell, including both ionic and electronic mechanisms of conduction. Here, we preferred to use a value obtained experimentally from the impedance spectra of the simulated cell [7]: values in the order of 0.27–0.43 Ω cm^2 have been derived.

Activation losses

Activation losses are related to the energy barrier that the reactive species must overcome in order to sustain the reaction. Activation polarization is usually described by the Butler–Volmer equation [38,39]:

$$J = J_0\left\{\exp\left(\beta\frac{n_eF\eta_{ACT}}{R_gT}\right) - \exp\left(-(1-\beta)\left(\frac{n_eF\eta_{ACT}}{R_gT}\right)\right)\right\} \quad (12)$$

As suggested in literature [40], when the charge transfer reaction is assumed to be a one-step single electron transfer process, the hyperbolic sine formula is a good approximation of the Butler–Volmer equation: such an equation can be further simplified for the case $\beta = 0.5$ to become [38]:

$$\eta_{ACT} = \frac{2R_gT}{n_eF}\sinh^{-1}\left(\frac{J}{2J_0}\right) \quad (13)$$

The exchange current density J_0 represents the equilibrium electron flow from cathode to anode and vice versa, and is calculated from the Arrhenius law [41] at the anode (Eq. (14)) and cathode (Eq. (15)) respectively.

$$J_0^{Anode} = \gamma^{Anode}\left(\frac{P_{H_2}}{P_{Ref}}\right)\left(\frac{P_{H_2O}}{P_{Ref}}\right)\exp\left(-\frac{E_A^{Anode}}{R_gT}\right) \quad (14)$$

$$J_0^{Cathode} = \gamma^{Cathode}\left(\frac{P_{O_2}}{P_{Ref}}\right)^{0.25}\exp\left(-\frac{E_A^{Cathode}}{R_gT}\right) \quad (15)$$

The values of the pre-exponential coefficients γ and the activation energies E_A^{Anode} and $E_A^{Cathode}$ are specified in Table 3.

Concentration losses

Concentration losses are related to the mass transfer resistance of the reacting species within the pores of the electrodes. Reacting species have to diffuse through the pores of the electrodes to reach the sites where the electrochemical reaction takes place. Low gas concentration in the pores of the electrodes may limit the current and cause an increase of polarizations. In agreement with literature [42], the concentration polarization is calculated as follows:

$$\eta_{CONC} = \frac{R_gT}{n_eF}\ln\left(1-\frac{J}{J_{lim}}\right) \quad (16)$$

The limiting current density J_{lim} is referred to as the maximum current density achieved in the case of complete reaction of the hydrogen present in the anode chamber. It depends both on molecular and Knudsen diffusion coefficients of the reactive species [38], and it is a function of the porosity, tortuosity and thickness of the electrode.

In this model, the value of the limiting current density J_{lim} was just a rough estimation (see Table 3). However, the experimental tests were performed in the low to medium current density region, where the concentration losses are expected to be limited, as witnessed by the shape of the experimental curves in all the tested conditions (see Figs. 6–8 below).

Table 3 – Input data for the SOFC model.

Parameter	Value	Reference
E_A^{Anode} [J mol^{-1}]	$1.05\cdot10^5$	[48]
$E_A^{Cathode}$ [J mol^{-1}]	$1.10\cdot10^5$	[48]
γ^{Anode} [A m^{-2}]	$1.34\cdot10^{10}$	[48]
$\gamma^{Cathode}$ [A m^{-2}]	$2.05\cdot10^9$	[48]
J_{lim} [A m^{-2}]	20,000	–
β [–]	0.5	–
F [C mol^{-1}]	96,485	–
R_g [J K^{-1} mol^{-1}]	8.314	–
T [K]	1073	–
P_{Ref} [bar]	1.013	–

Furnace model

A thermal furnace is used for the combustion of the outlet stream from the anodic chamber of the SOFC. The energy released in such combustion is then valorized for the preheating of the inlet streams (biogas, air to SOFC, and water). An ad-hoc model was adopted for the simulation of the furnace; for this purpose the DSMOKE software [43] has been used. The DSMOKE software, developed at Politecnico di Milano, is a well-tested code [44,45] which uses a detailed kinetic scheme for the simulation of non-ideal chemical reactors, and can include more than 500 species and 30,000 reactions. It is characterized by generality and modularity so as to allow the possibility to select a reduced number of chemical kinetics schemes according to the system to be modelled. Moreover, it allows to model series of ideal reactors in order to represent with higher accuracy and without any computational fluid dynamics study complex and non-ideal industrial systems thanks to appropriate combinations of ideal steps. In the specific case of the paper, the reactor selected for the simulation is a non-isothermal plug-flow reactor operating at atmospheric pressure with a volume equal to $5\cdot10^{-4}$ m^3, and the selected kinetic scheme includes only few families of reactions (hydrogen-oxygen, light hydrocarbons, oxidation), which allows to keep computational effort small.

As in acquaintance of the authors, the DSMOKE was never included in simulations at the process scale and its integration required the development of dedicated files and tools ac-cording to OPC (OLE for Process Control) directives. Microsoft Excel was adopted as hub for all the information of the different tools and models adopted (Fig. 2). PRO/II communi-cate with MS Excel thanks to ad hoc macros predisposed to exchange information with external simulation environments [46]. MS Visual C++ model for the SOFC and DSMOKE Suite communicate with MS Excel by means of I/O (Input/Output) ASCII files and special functions to read and write the exchanged information. Petri network techniques [47] are adopted to prevent any transmission problem.

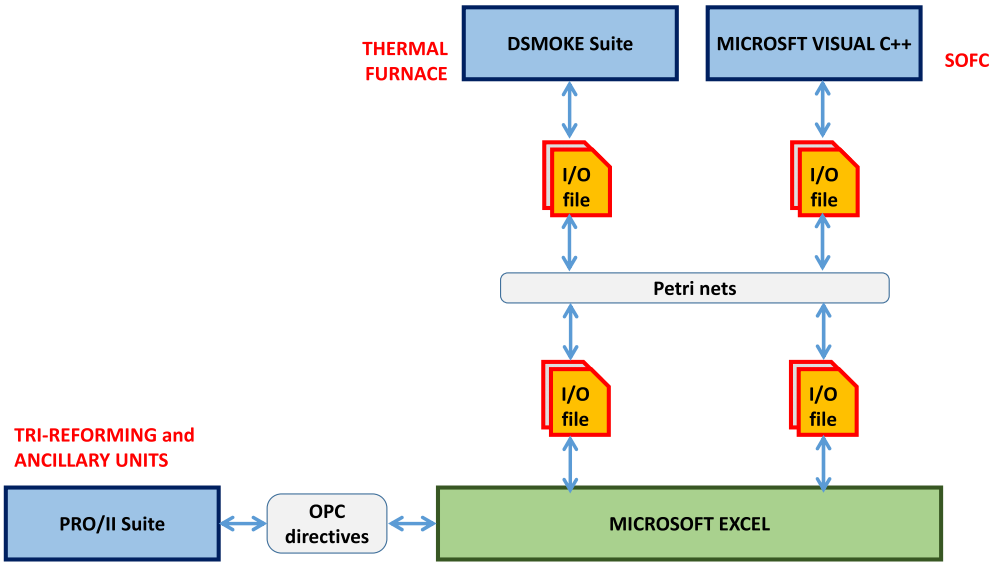

Fig. 2 – Model integration via Microsoft Excel as information hub for process computing.

Results and model validation

The available experimental data at the selected operative condition [7] allowed to validate the models developed in the simulation of the system. In particular, the results obtained from the simulation of the tri-reforming model, the SOFC model, and the overall combined process model were compared. Such comparisons are described in the following sections.

Tri-reforming model

Four experimental tests, at different temperatures, were carried out in order to validate the tri-reforming model used in the simulation at a wide-range conditions. The selected temperatures were 795 °C, 840 °C, 900 °C and 950 °C. The assumption of isothermal operation and quasi-equilibrium conditions have been modelled using the so-called temperature approach of PRO/II (with a temperature in the order of 10 °C less than the experimental temperature), which is well-established in the process simulation of such systems.

In Fig. 3 and Fig. 4 the outlet molar composition obtained by the model (described in paragraph 'Tri-reformer model' above) and the experimental values are shown in a wide range of temperatures. There is a good agreement between the model and the experimental data, with the exception of the water mole fraction that seems to be underestimated by the model. However, this may be due to an inaccurate experimental evaluation of such low concentrations of water.

The conversion profiles of CO_2 and CH_4 from both experimental and model data are shown in Fig. 5. As expected from the thermodynamic equilibrium, an increase in temperatures is beneficial for the two endothermic reactions (DR and SR) causing a higher conversion of CH_4 and CO_2.

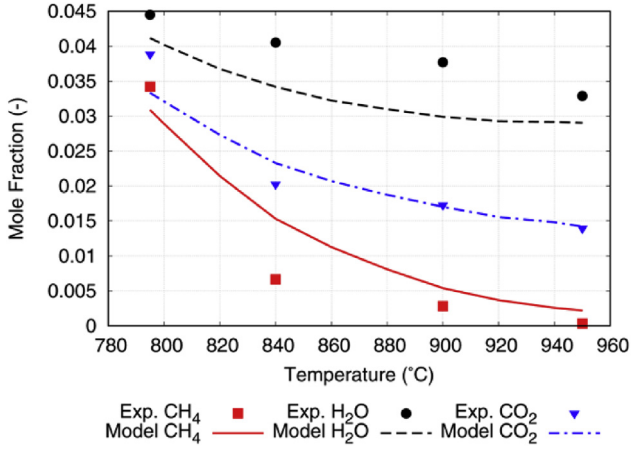

Fig. 3 – CH_4, H_2O and CO_2 outlet molar composition for the tri-reforming process; experimental and model values.

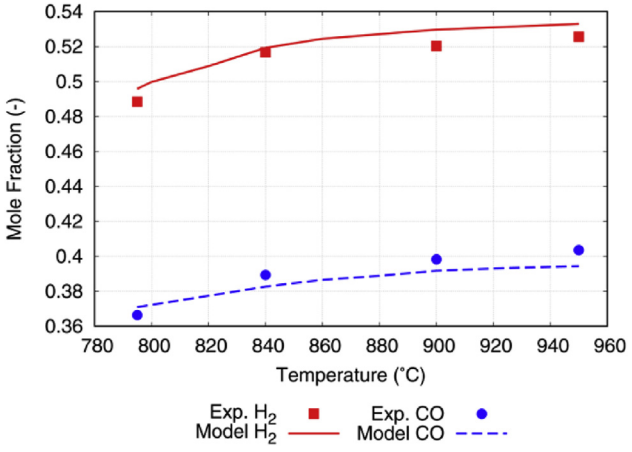

Fig. 4 – H_2 and CO outlet molar composition for the tri-reforming process; experimental and model values.

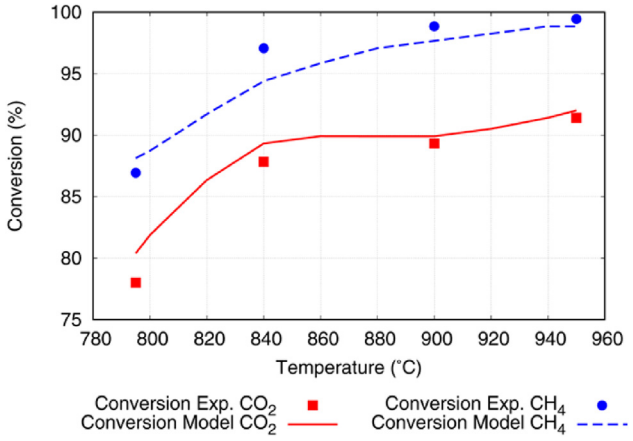

Fig. 5 – Conversion profiles for CO_2 and CH_4: experimental and model values.

Subsequently, several tests (ranging from #1 to #9) with different inlet compositions were carried out at a fixed temperature (800 °C). Table 1 shows the CO and H_2 outlet composition obtained in the experimental tests compared with those obtained by the model; for each test, the gap between these values is less than 4%.

Complete data regarding the conversion of methane and carbon dioxide are shown in Table 2. Also in this case the experimental and model values are in very good agreement for each test, with differences lower than 4%. Therefore, the Gibbs reactor is able to predict the tri-reforming process outcome with appropriate accuracy, demonstrating that it operates at thermodynamic equilibrium.

SOFC model

The fuel cell model has been validated by using the available experimental data. A comparison between the experimental and calculated polarization curves, for each of the considered tests, was assessed.

The polarization curves for tests #1, #2 and #3 (see Table 1 for test specifications) are shown in Fig. 6. The model plot agrees quite well with the experimental curve in the whole data range, except for a significant difference in proximity of the open circuit voltage (OCV); this discrepancy is accounted for by the simplifications introduced in the Butler–Volmer equation. Nonetheless, such a deviation is within a region where conventionally the fuel cell does not operate. Analogous results are observed in different conditions and are reported in Fig. 7 and Fig. 8.

Another offset between the experimental and model data (see Fig. 7, in particular) is that the modelled curves are mostly shifted at slightly lower potentials respect to the experimental data in the region dominated by the ohmic polarization. This behaviour arises from difficulties in evaluating the exact ohmic losses within the cell, whose resistance has been extrapolated from the experimental impedance spectra at 0.8 V. A particularly evident deviation between data and model results is observed in test #9 (see Fig. 8c), when a low

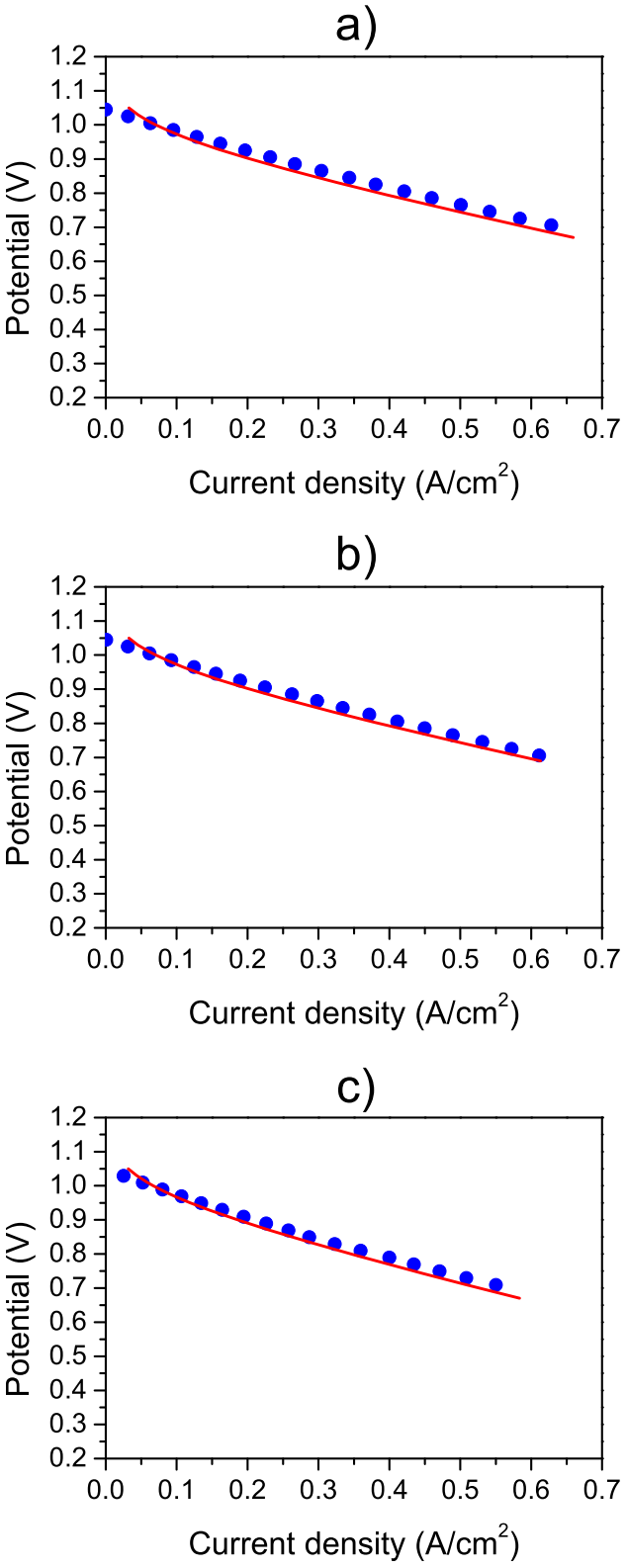

Fig. 6 – Polarization curves for a) Test #1; b) Test #2 and c) Test #3. Symbols (●) represents experimental data. Solid line (——) represents model data.

methane conversion is obtained in the tri-reforming process. In this case a fast deactivation of the Ni-based anode may be predicted, due to the formation of carbonaceous deposits inside the pores of the electrodes, that can lead to its partial or

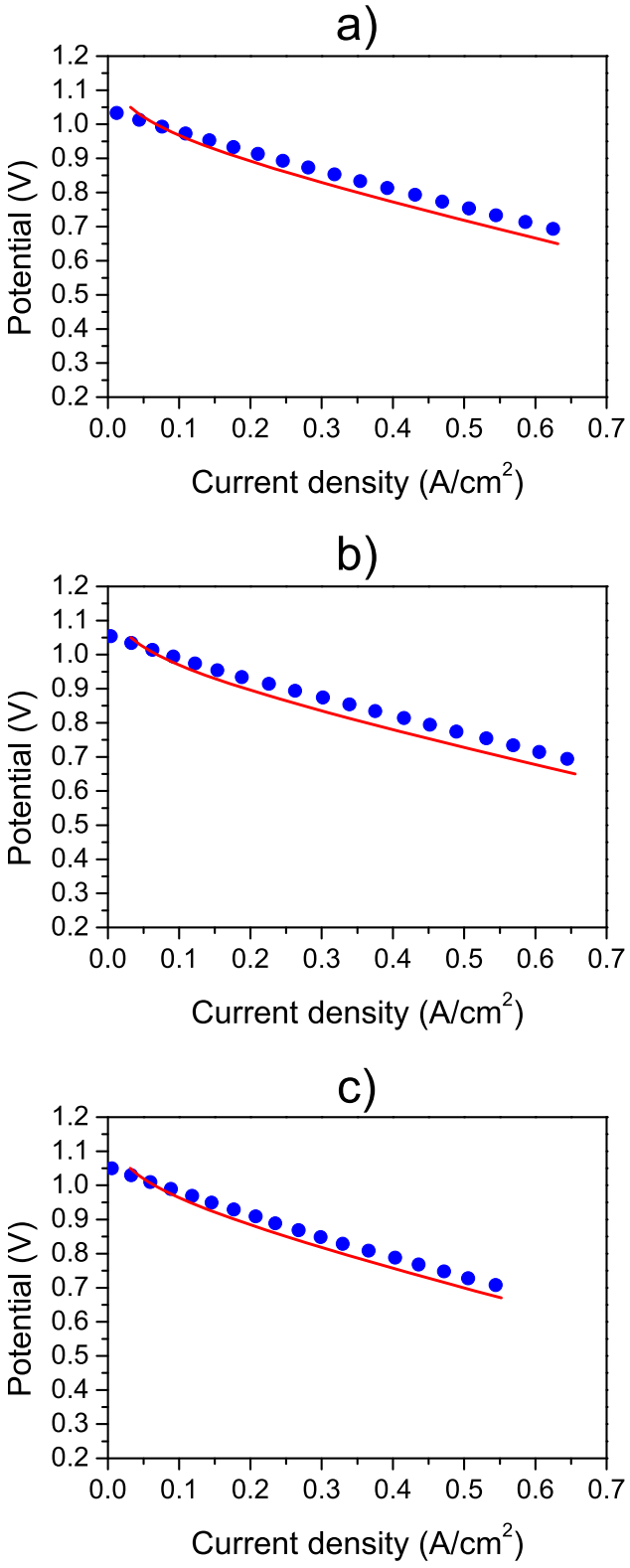

Fig. 7 – Polarization curves for a) Test #4; b) Test #5 and c) Test #6. Symbols (●) represents experimental data. Solid line (——) represents model data.

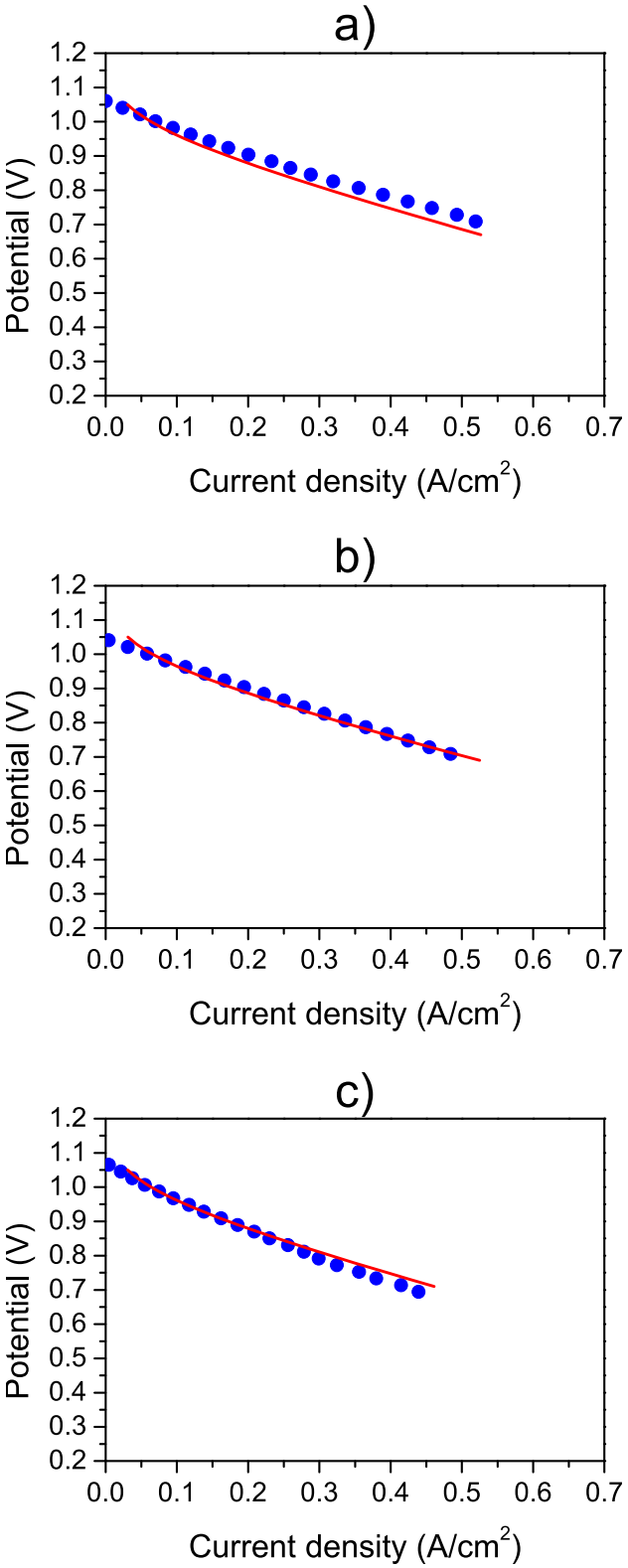

Fig. 8 – Polarization curves for a) Test #7; b) Test #8 and c) Test #9. Symbols (●) represents experimental data. Solid line (——) represents model data.

total occlusion [7]; therefore, a decrease of the cell efficiency in the experimental curves is reasonable, but cannot be taken into consideration by the model, leading to an overestimation of the cell voltage.

Process-scale performance

Once the model was validated, the overall system (described in paragraph 'Combined tri-reformer/SOFC process

Table 4 – Comparison of current density obtained by model and experimental values (@ 0.8 V).

Test	Exp. current density [A cm^{-2}]	Model current density [A cm^{-2}]	Error [%]
#1	0.42	0.41	2.38
#2	0.41	0.40	2.44
#3	0.36	0.35	2.78
#4	0.43	0.39	9.30
#5	0.45	0.41	8.89
#6	0.37	0.35	5.41
#7	0.35	0.33	5.71
#8	0.34	0.35	2.94
#9	0.30	0.32	6.67

modelling' above) was assessed and simulated with the conditions equal to those developed during the experimental tests, i.e. biogas flow into the tri-reforming reactor at a rate of 100 $cm^3\ min^{-1}$ and SOFC potential fixed to 0.8 V. Table 4 shows the current density error between the model and the experimental data. For each test the error was below the 10%, that may be considered reasonable since it is of the same order of the experimental error.

It is noteworthy that the current density, and hence the cell performance, decreases with the gradual decrease of CH_4 conversion; thus, supporting the fact that the formation of carbon deposits may depress the charge transfer process by poisoning the sites inside the porous electrode.

The utilization factor (u) of a fuel cell is defined as the ratio between the fuel consumed and the fuel provided to the cell.

$$u = \frac{F^{cell}_{H_2,i} - F^{cell}_{H_2,o}}{F^{cell}_{H_2,i}} \tag{17}$$

The utilization factor has a big influence on the cell efficiency; in fact, according to Wen et al. [49], when dealing with the optimization of solid oxide fuel cells the utilization factor is a key parameter, together with the cell configuration.

Low values of utilization factor (in the range of about 5–7%) were obtained, as shown in Table 5. These values were expected to be due to the size of the system: in fact, the fuel provided to the cell is almost ten times those predictable from the Faraday's equation. Additionally, the slight variation of the utilization factor – in each of the tests – cannot be attributed to the variation of the hydrogen concentration, that is almost constant (see Table 1) in all tests. Thus, the change in the ohmic losses is responsible of the reduction of the utilization factor; indeed, increasing ohmic losses causes a decrease in current density, and therefore reduces the amount of hydrogen converted into the cell. As a result, the efficiency of the fuel cell is very low (~2.5%) and, despite the introduction of heat recovery units and other power generation systems (such as the turbine) downstream, the overall performance of the system is also very low (efficiency ~4%).

Table 5 – Cell utilization factor and hydrogen inlet and outlet composition.

Test	u [%]	Inlet H_2 composition [mol]	Outlet H_2 composition [mol]
#1	6.82	0.52	0.49
#2	6.76	0.53	0.49
#3	6.02	0.53	0.50
#4	6.06	0.53	0.49
#5	6.01	0.53	0.50
#6	4.96	0.54	0.51
#7	5.29	0.53	0.50
#8	5.59	0.53	0.50
#9	5.26	0.53	0.50

Although the modelling of a real system is out of the scope of the present study, due to the characteristic and size of the equipment used for the experimental tests, the developed model could be easily applied to larger systems with only minimal modifications. Moreover, it could be helpful in studying system feasibility and optimization assessment, in order to increase the overall system performance.

Conclusions

The urgency to explore alternative energy sources not dependent on fossil fuels, the rising concern in environmental issues altogether with the usual interest in economic growth have encouraged the investigation of new technologies based on renewable fuels. One way to tackle such issues is through the use of biofuels, such as biomass or biogas, and the integration of chemical processes to decrease emissions while increasing energy efficiency and profitability of the process. Thus, we have presented a first development of a model of an integrated tri-reformer/SOFC system based on biogas for the production of sustainable and clean energy. Such a process appears to be a promising approach to contribute in the reduction of carbon footprint, in comparison with the usual power generation systems based on the combustion of fossil fuels. The proposed model, validated with experimental data, has the ability to reproduce a micro-scale plant quite accurately under a variety of conditions, resulting in a flexible solution capable of being scaled-up to the study of larger systems.

Nomenclature

E_A^{Anode}	activation energy for reaction in anode, J mol^{-1}
$E_A^{Cathode}$	activation energy for reaction in cathode, J mol^{-1}
$F^{cell}_{i,i}$	inlet molar flow of species i to the fuel cell, mol s^{-1}
$F^{cell}_{i,o}$	outlet molar flow of species i to the fuel cell, mol s^{-1}
F	Faraday constant, A s mol^{-1}
ΔG_{rxn}	change of reaction's Gibbs free energy, J mol^{-1}
J	current density, A m^{-2}
J_o	exchange current density, A m^{-2}
J_{lim}	limiting current density, A m^{-2}
n_e	number of reacting electrons, –
P_i	partial pressure of species i, Pa
P_{Ref}	reference pressure, Pa
R_g	universal gas constant, J mol^{-1} K^{-1}
T	temperature, K
η_{ACT}	activation polarization, V
η_{CONC}	concentration polarization, V
η_{OHM}	ohmic polarization, V
V_{OP}	operative voltage, V
V_{REV}	reversible potential of the cell (OCV), V

Greek letters

β	transfer coefficient, –
γ	pre-exponential factor for reaction in electrode, A m^{-2}

REFERENCES

[1] Ediger VŞ, Hoşgör E, Sürmeli AN, Tatlıdil H. Fossil fuel sustainability index: an application of resource management. Energy Policy 2007;35:2969–77.

[2] Dunn S. Hydrogen futures: toward a sustainable energy system. Int J Hydrogen Energy 2002;27:235–64.

[3] Ball M, Wietschel M. The future of hydrogen – opportunities and challenges. Int J Hydrogen Energy 2009;34:615–27.

[4] Winter CJ. Hydrogen energy – abundant, efficient, clean: a debate over the energy-system-of-change. Int J Hydrogen Energy 2009;34:S1–52.

[5] Effendi A, Zhang ZG, Hellgardt K, Honda K, Yoshida T. Steam reforming of a clean model biogas over Ni/Al_2O_3 in fluidized- and fixed-bed reactors. Catal Today 2002;77:181–9.

[6] Edelmann W. Biogas production and usage. In: Kaltschmitt M, Hartmann H, editors. Energy from biomass: basic principles, technologies and processes. Leipzig, Germany: Springer; 2001.

[7] Lo Faro M, Vita A, Pino L, Aricò AS. Performance evaluation of a solid oxide fuel cell coupled to an external biogas tri-reforming process. Fuel Process Technol 2013;115:238–45.

[8] Van Herle J, Membrez Y, Bucheli O. Biogas as a fuel source for SOFC co-generators. J Power Sources 2004;127:300–12.

[9] Xuan J, Leung MKH, Leung DYC, Ni M. A review of biomass-derived fuel processors for fuel cell systems. Renew Sustain Energy Rev 2009;13:1301–13.

[10] Larminie J, Dicks A. Fuel cell systems explained. J. Wiley; 2003.

[11] EG & G Technical Service I. Fuel cell handbook. 7th ed. US Department of Energy; 2004.

[12] Papadias DD, Ahmed S, Kumar R. Fuel quality issues with biogas energy – an economic analysis for a stationary fuel cell system. Energy 2012;44:257–77.

[13] Ballarini AD, De Miguel SR, Jablonski EL, Scelza OA, Castro AA. Reforming of CH_4 with CO_2 on Pt-supported catalysts: effect of the support on the catalytic behaviour. Catal Today 2005;107–108:481–6.

[14] Joensen F, Rostrup-Nielsen JR. Conversion of hydrocarbons and alcohols for fuel cells. J Power Sources 2002;105:195–201.

[15] Serrano-Lotina A, Rodríguez L, Muñoz G, Daza L. Biogas reforming on La-promoted NiMgAl catalysts derived from hydrotalcite-like precursors. J Power Sources 2011;196:4404–10.

[16] Piroonlerkgul P, Assabumrungrat S, Laosiripojana N, Adesina AA. Selection of appropriate fuel processor for biogas-fuelled SOFC system. Chem Eng J 2008;140:341–51.

[17] Specchia S, Negro G, Saracco G, Specchia V. Fuel processor based on syngas production via short contact time catalytic partial oxidation reactors. Appl Catal B Environ 2007;70:525–31.

[18] Lau CS, Tsolakis A, Wyszynski ML. Biogas upgrade to syn-gas (H_2–CO) via dry and oxidative reforming. Int J Hydrogen Energy 2011;36:397–404.

[19] Pino L, Vita A, Cordaro M, Recupero V, Hegde MS. A comparative study of Pt/CeO_2 catalysts for catalytic partial oxidation of methane to syngas for application in fuel cell electric vehicles. Appl Catal A General 2003;243:135–46.

[20] Christian Enger B, Lødeng R, Holmen A. A review of catalytic partial oxidation of methane to synthesis gas with emphasis on reaction mechanisms over transition metal catalysts. Appl Catal A General 2008;346:1–27.

[21] Song C, Pan W. Tri-reforming of methane: a novel concept for catalytic production of industrially useful synthesis gas with desired H_2/CO ratios. Catal Today 2004;98:463–84.

[22] Izquierdo U, Barrio VL, Requies J, Cambra JF, Güemez MB, Arias PL. Tri-reforming: a new biogas process for synthesis gas and hydrogen production. Int J Hydrogen Energy 2013;38:7623–31.

[23] Manenti F, Leon-Garzon AR, Ravaghi-Ardebili Z, Pirola C. Systematic staging design applied to the fixed-bed reactor series for methanol and one-step methanol/dimethyl ether synthesis. Appl Therm Eng 2014;70(2):1228–37.

[24] Pirola C, Scavini M, Galli F, Vitali S, Comazzi A, Manenti F, et al. Fischer-Tropsch synthesis: EXAFS study of Ru and Pt bimetallic Co based catalysts. Fuel 2014;132:62–70.

[25] Nawfal M, Gennequin C, Labaki M, Nsouli B, Aboukaïs A, Abi-Aad E. Hydrogen production by methane steam reforming over Ru supported on Ni-Mg-Al mixed oxides prepared via hydrotalcite route. Int J Hydrogen Energy 2014;40:1269–77.

[26] Pino L, Vita A, Laganà M, Recupero V. Hydrogen from biogas: catalytic tri-reforming process with Ni/LaCeO mixed oxides. Appl Catal B Environ 2014;148–149:91–105.

[27] Tomishige K, Chen YG, Fujimoto K. Studies on carbon deposition in CO_2 reforming of CH_4 over nickel-magnesia solid solution catalysts. J Catal 1999;181:91–103.

[28] Tsipouriari VA, Verykios XE. Carbon and oxygen reaction pathways of CO_2 reforming of methane over Ni/La_2O_3 and Ni/Al_2O_3 catalysts studied by isotopic tracing techniques. J Catal 1999;187:85–94.

[29] Vita A, Pino L, Cipitì F, Laganà M, Recupero V. Biogas as renewable raw material for syngas production by tri-reforming process over $NiCeO_2$ catalysts: optimal operative condition and effect of nickel content. Fuel Process Technol 2014;127:47–58.

[30] Trendewicz AA, Braun RJ. Techno-economic analysis of solid oxide fuel cell-based combined heat and power systems for biogas utilization at wastewater treatment facilities. J Power Sources 2013;233:380–93.

[31] Chiodo V, Galvagno A, Lanzini A, Papurello D, Urbani F, Santarelli M, et al. Biogas reforming process investigation for SOFC application. Energy Convers Manage 2015;98:252–8.

[32] Lanzini A, Leone P. Experimental investigation of direct internal reforming of biogas in solid oxide fuel cells. Int J Hydrogen Energy 2010;35:2463–76.

[33] Göll S, Samsun RC, Peters R. Analysis and optimization of solid oxide fuel cell-based auxiliary power units using a generic zero-dimensional fuel cell model. J Power Sources 2011;196:9500–9.

[34] Anderson T, Vijay P, Tade MO. An adaptable steady state Aspen Hysys model for the methane fuelled solid oxide fuel cell. Chem Eng Res Des 2014;92:295–307.

[35] Amiri A, Vijay P, Tadé MO, Ahmed K, Ingram GD, Pareek V, et al. Solid oxide fuel cell reactor analysis and optimisation through a novel multi-scale modelling strategy. Comput Chem Eng 2015;78:10–23.

[36] Towler G, Sinnott RK. Chemical engineering design: principles, practice and economics of plant and process design. Elsevier Science; 2007.

[37] Soave G. Equilibrium constants from a modified Redlich-Kwong equation of state. Chem Eng Sci 1972;27:1197–203.

[38] Chan SH, Khor KA, Xia ZT. A complete polarization model of a solid oxide fuel cell and its sensitivity to the change of cell component thickness. J Power Sources 2001;93:130–40.

[39] Zhu H, Kee RJ, Janardhanan VM, Deutschmann O, Goodwin DG. Modeling elementary heterogeneous chemistry and electrochemistry in solid-oxide fuel cells. J Electrochem Soc 2005;152:A2427–40.

[40] Noren DA, Hoffman MA. Clarifying the Butler-Volmer equation and related approximations for calculating activation losses in solid oxide fuel cell models. J Power Sources 2005;152:175–81.
[41] Calise F, Dentice d'Accadia M, Palombo A, Vanoli L. One-dimensional model of a tubular solid oxide fuel cell. J Fuel Cell Sci Technol 2008:5.
[42] Gebregergis A, Pillay P. The development of solid oxide fuel cell (SOFC) emulator. In: Power Electronics Specialists Conference; 2007. p. 1232–8. PESC 2007 IEEE2007.
[43] Manca D, Buzzi-Ferraris G, Faravelli T, Ranzi E. Numerical problems in the solution of oxidation and combustion models. Combust Theory Model 2001;5:185–99.
[44] Ranzi E, Corbetta M, Manenti F, Pierucci S. Kinetic modeling of the thermal degradation and combustion of biomass. Chem Eng Sci 2014;110:2–12.
[45] Manenti F, Papasidero D, Bozzano G, Ranzi E. Model-based optimization of sulfur recovery units. Comput Chem Eng 2014;66:244–51.
[46] Manenti F, Signor S, Grottoli MG, Fabbri P. Adaptive data reconciliation coupling C++ and PRO/II and on-line application by the field. Computer Aided Chemical Engineering; 2010. p. 373–8.
[47] Reisig W. Petri nets and algebraic specifications. Theor Comput Sci 1991;80:1–34.
[48] Suther T, Fung A, Koksal M, Zabihian F. Macro level modeling of a tubular solid oxide fuel cell. Sustainability 2010;2:3549–60.
[49] Wen H, Ordonez JC, Vargas JVC. Optimization of single SOFC structural design for maximum power. Appl Therm Eng 2013;50:12–25.